Journal of Alloys and Compounds 647 (2015) 558–565

Contents lists available at ScienceDirect

Journal of Alloys and Compounds

journal homepage: http://www.elsevier.com/locate/jalcom

Evolution of room temperature ferromagnetism with increasing 1D growth in Ni-doped ZnO nanostructures

Bappaditya Pal [a], Soumen Dhara [b, 1], P.K. Giri [b], D. Sarkar [a, *]

[a] Department of Physics, Gauhati University, Guwahati 781014, India
[b] Department of Physics, Indian Institute of Technology Guwahati, Guwahati 781039, India

ARTICLE INFO

Article history:
Received 9 April 2015
Received in revised form
27 April 2015
Accepted 2 May 2015
Available online 10 June 2015

Keywords:
ZnO nanoparticles
Nanorods
Ni doping
Ferromagnetism
Photoluminescence
Defects
DMS

ABSTRACT

$Zn_{1-x}Ni_xO$ ($x = 0$, 0.03, and 0.5) 1D nanostructures showing room temperature ferromagnetism (RT FM) with high moment have been synthesized by a solvothermal route. X-ray diffraction, transmission electron microscopy (TEM), energy dispersive X-ray spectrum (EDS) and X-ray photoelectron spectroscopy (XPS) analysis reveal the growth of single phase wurtzite structure $Zn_{1-x}Ni_xO$ NRs of diameter 60–70 nm and length of 0.4–0.6 μm with the successful incorporation of Ni ions inside ZnO matrix. High resolution TEM lattice images show that all the NRs are single crystalline with a d-spacing of 2.57 Å with c-axis growth. Room temperature magnetic measurements exhibit strong ferromagnetic characteristic with magnetic moment of 1.13 emu/g, coercivity of 150 G. Photoluminescence (PL) spectra exhibit near band edge UV emission as well as defect related visible emission which is expected to play a significant role in the FM ordering, also PL spectra reveal slight band edge modification due to doping effect. Systemic structural, magnetic, and optical properties reveal that both the nature of the defects as well as Ni^{2+} ions are significant ingredients to attain FM characteristics with high moment and ordering temperature in the 1-dimensional ZnO NRs. Magnetic interaction is analysed using a bound magnetic polaron model and expected to arise from the intrinsic exchange interaction of Ni ions, Zn vacancy and O iterstitial related defects.

1. Introduction

Over the past decade, there has been tremendous interest in understanding the origin of room temperature ferromagnetism found in a variety of semiconductor oxides. Among them transition metal (TM) doped ZnO based diluted magnetic semiconductors (DMS) are potential candidate for the attainment of ferromagnetic ground state with a high (RT and above) Curie (T_C) temperature, following the theoretical prediction of room-temperature ferromagnetism (RTFM) in Mn doped ZnO [1–3]. It leads to a novel behavior for the use of both charge and spin of electrons by producing spin polarized carriers having promising prospect of applications in semiconductor spintronic devices [3–7]. The coexistence of magnetic, semiconducting, and optical functionalities increase the potential of TM-doped ZnO (ZnO:TM) to be a multifunctional material [3,5]. It might have potential applications in the new emerging field of optoelectronics, spin polarized light emitting diodes, magnetic tunnel junctions, photovoltaics and sensors [4,8,9]. Further, among the II–VI semiconductors, ZnO is a versatile multifunctional candidate, with a direct wide band gap (3.37 eV at 300 K), large excitonic binding energy (60 meV), outstanding electro-optic, piezoelectric properties, and excellent chemical stability which can be useful in electronics and optoelectronics [10,11].

There are debates regarding the origin of FM, kind of interaction and the role of TM in ZnO based DMSs. Various studies indicate the origin of FM as intrinsic in nature and is due to the exchange interaction between the localized magnetic moment of TM ion and delocalized charge carriers [1], or through the percolation of defect mediated bound magnetic polarons (BMP), formed by the intrinsic defects, related to vacancy or interstitials [12,13]. However, in some cases, it is reported that FM is extrinsically originated from segregation of TM ions or from the secondary magnetic phases [14,15]. Also sometimes defect densities, such as oxygen/zinc vacancies or interstitials [16,17] and cluster of defects [18] could alone trigger FM (d_0 FM) without TM doping. However, in case of d_0 FM, for most of

* Corresponding author.
E-mail addresses: bpal.iitg@gmail.com (B. Pal), sarkardeepali@gmail.com (D. Sarkar).
[1] Present address: Department of Electrical and Electronic Engineering, Graduate School of Engineering, Kobe University, 1-1 Rokkodai, Nada, Kobe 657–8501, Japan.

http://dx.doi.org/10.1016/j.jallcom.2015.05.218
0925-8388/

these materials it is difficult to retain FM at elevated temperatures. Also, it is very difficult to establish a direct link between the magnetization and defects due to complexity of defect states in ZnO and to have its suitable handling for the device application purpose. Hence, the conclusive origin of RTFM is yet to be uncovered, and the mechanism behind the magnetic ordering is still under debate.

The attainment of HTFM, its stability and reproducibility in various environments is one of the challenging issues in these systems. Researchers have tried to synthesize Ni doped ZnO based DMSs, mostly in thin films and by various sol-gel reaction routes. Liu et al. observed the RTFM behavior in Ni-doped ZnO films synthesized by pulsed laser deposition [19]. Gunjan etal. have found RT FM with low moment in Ni doped ZnO Nanoparticles (NPs) by a sol-gel route [20]. Satyarthi etal. have reported the coexistence of intrinsic and extrinsic origins of RT FM in Ni ion implanted ZnO films [21]. Also, it has been reported that the nature of FM in Ni doped ZnO does not remain intrinsic upon annealing in various environments at high temperature because of segregation of TM ions [22]. Singhal et al. reported that FM in hydrogenated and vacuum annealed Ni doped ZnO disappears upon long reheating in air at very high temperatures of 700 C and 800 C respectively [23].

The kind of FM interaction with respect to the experimental findings have been little explored in Ni doped ZnO systems as compared to the Co doped ZnO systems. Moreover, synthesis of Ni doped ZnO nanostructures (NS) showing FM above room temperature with a high moment and high crystallinity still remains a significant challenge for future spintronic devices. Under this scenario, magnetism in Ni doped ZnO is still a subject of much interest that demands careful investigations. In this paper, we have followed an easy approach toward the synthesis of long and uniform $Zn_{1-x}Ni_xO$ Nanostructures by a solvothermal route at ambient conditions. Synthesis by solvothermal route using autoclave offers better advantages, such as easy and effective control of synthesis parameters, like low synthesis temperature, short-long reaction time, low cost processing, economical, and environmentally kind too. The structural characterization and phase identification are carried out to check the phase identification, morphology and elemental composition. Optical measurements are carried out to check the elemental ionic states, doping related changes in band edge emission, the kind of defects present and their changes with doping. The magnetic properties are measured to find the M-H loop, order of magnetic moment and its nature.

2. Experimental details

2.1. Synthesis of nanorods

$Zn_{1-x}Ni_xO$ (x = 0, 0.03, 0.05, molar percentage) NSare synthesized by a sovothermal route. Zinc acetate dihydrate($Zn(Ac)_2$, $2H_2O$) and Nickel acetate tetra hydrate ($Ni(Ac)_2$,$4H_2O$) of analytic grade and sodium hydroxide (NaOH) pellets (Merck) are used for the synthesis of undoped and doped ZnO NPs/NRs. Distilled deionized (DI) water is used during all the experiments. In a typical synthesis, ($Zn(Ac)_2$, $2H_2O$) and ($Ni(Ac)_2$, $4H_2O$) of different molar percentages are mixed with 50 ml DI water with continuous stirring for 1 h. Next the solution mixture is transferred into Teflon-lined autoclave (Berghof, BR- 100) of 100 ml capacity. Then 25 ml NaOH solution (1 M) is drop wise added with increasing temperature upto 90 °C in few steps, under continuous stirring. The reaction rate affects the growth morphology of the samples. We carefully observe that this kind of slow reaction have tendency for the TM ions to insert inside the ZnO matrix and distribute quite well, forming 1D NR type structure. While just mixing the precipitates all together and heating have chances to produce arbitrary shaped NP structure or TM related secondary phases. Next the chamber is closed and the mixture is heated at different temperatures (120–150) °C for 10–20 h and then cooled down to RT naturally. The precipitates are collected, alternately washed with deionized water and ethanol for several times till the pH~7 is reached and finally dried in room temperature. The undoped ZnO NPs and 3%, 5% Ni doped ZnO NPs, NRs for reaction temperatures of (120–150 C) and reaction time of (10–20) h are named as 0-ZnO-NPs, 1-ZnO-NPs, 2-ZnO-NPs, 3-ZnO-NRs respectively for convenience and details are mentioned in Table 1.

2.2. Characterization

The phase purity and crystal structure of the $Zn_{1-x}Ni_xO$ samples are characterized by X-ray diffraction (XRD) (Rigaku RINT 2500 TTRAX-III, Cu K radiation). The morphology of the samples are identified using a field emission scanning electron microscopy (FESEM) (Sigma, Zeiss). The high magnification surface morphologies are studied by transmission electron microscopy (TEM), high-resolution TEM (HRTEM), selected area electron diffraction (SAED) pattern and energy dispersive X-ray spectrum (EDS) (JEOL-JEM 2010 operated at 200 kV). The room temperature PL spectra of all the samples were recorded with a 325 nm He-Cd laser excitation using a commercial PL spectrometer (Flurolog-3, Horiba) equipped with a PMT(photo multiplier tube) (detector excitation, emission slit width-2 nm, integration time-1sec and emitted PL collected through a 350 nm high bandpass filter). The magnetic properties of the samples are examined by using a Lakeshore vibrating sample magnetometer (VSM) (Model no. 7410). X-ray photoelectron microscopy (XPS) measurement was carried out with a fully automated XPS microprobe (PHI X-tool, ULVAC-PHI) using Al K_α x-ray beam (1486.7 eV) with beam current of 5 mA. Carbon 1s spectrum is used for the calibration of the XPS spectra recorded for various samples.

3. Results and discussion

3.1. Microstructureand morphology

Fig. 1(a–d) shows a typical XRD pattern for the $Zn_{1-x}Ni_xO$ (x = 0, 0.03, 0.05) samples with respect to different morphology and synthesis conditions. Observed peaks confirm the single crystalline ZnO wurtzite structure for the pure ZnO NPs and Ni doped ZnO NPs, NRs. One small intensity secondary phase related peak can be seen for the 1-ZnO NPs for lower reaction temperature of synthesis. It may appear due to some Ni nanoclusters or $Ni(OH)_3$ related phases. Overall crystallinity has been improved and the morphology has been changed from NPs to NRs with the increasing reaction temperature and time for the Ni doped samples. Also it shows clear shifting of the diffraction peaks towards the higher angle with doping for the three most intense peaks of the XRD pattern. The lattice parameters **a**, **c** and the cell volume **'v'** are calculated from the XRD peak positions and we find that lattice parameters have decreased with doping; as a consequence, the lattice volume decreases (details: in Table 1). This is consistent with the fact that the ionic radius of Ni^{2+} is 0.55 Å, whereas that of Zn^{2+} is 0.60 Å [24]. The shifting of XRD pattern and corresponding decrease of the lattice parameters suggest that Ni^{2+} ions are successfully incorporated into the ZnO lattice at the Zn^{2+} sites.

The general morphologies of the $Zn_{1-x}Ni_xO$ samples are shown in Fig. 2. Fig. 2(a) shows the FESEM image of undoped ZnO nanoparticles(NPs). Fig. 2 (b) & (c) show TEM images of the 3% and 5% Ni doped ZnO nanoparticles (NPs) of average sizes as 50–100 nm &200–300 nm respectively. Fig. 2 (d) shows TEM image of the 5% Ni doped ZnO NRs. TEM micrograph reveals clearly the formation of good quality Ni doped ZnO NRs having a smooth surface with

Table 1
Lattice parameters calculated from the XRD pattern; Elemental composition extracted from XPS spectra.

Sample type		Crystal structure from XRD						Elemental composition from XPS		
		2θ (degree)		FWHM (31)	Lattice constants			Zn at. %	O At. %	Ni at. %
					A (Å)	C (Å)	V (Å^3)			
Undoped ZnO	0-ZnO NPs	31.73	34.39	0.262	3.253	5.211	23.88	38	62	0
3%Ni-ZnO-120 C-10h-NPs	1-ZnO NPs	31.79	34.45	0.294	3.245	5.195	23.64	40.2	57	1.8
5%Ni-ZnO-120 C-15h-NPs	2-ZnO NPs	31.97	34.62	0.389	3.230	5.178	23.39	37	60.8	2.2
5%Ni-ZnO-150 C-20h-NRs	3-ZnO NRs	32.10	34.73	0.441	3.217	5.162	23.29	35	61.1	3.9

diameter of 60–70 nm and length of 0.4–0.6 μm. Note that the Ni doped samples for lower reaction temperatures and times are of rectangular shaped NPs. While, with the higher reaction temperature and time, morphology leads to the long 1D NRs due to C-axis growth, asfor the ZnO nanostructures C-axis exhibits the highest growth rate due to the structure and surface anisotropy [25]. The difference of the crystal growth velocities in different directions is expected to cause the change of morphologies as the surface energies are different for different crystal faces. Similar findings have been observed for Ce-doped ZnO NRs and Co doped ZnO NRs [26–28]. Also the accommodation of Ni ions along the C-axis enhances FM interaction in the TM doped ZnO NRs. HRTEM lattice images and the SAED pattern illustrate that all the NRs are single crystalline. The d-spacing of the crystal plane is calculated as 2.57 Å showing the preferable crystal growth plane (002). Energy-dispersive X-ray spectroscopy (EDS) analysis on a single NR confirms the presence of Niions in the ZnO matrix. EDS analysis shows 2.36 atomic % of Ni doping in the ZnO NRs, corresponding to the 5M molar percentage of the initial cationic precursor, with consideration of the accuracy of the EDS analysis. We also confirm the presence of substituted Niions inside the ZnO matrix by XPS analysis, as discussed below.

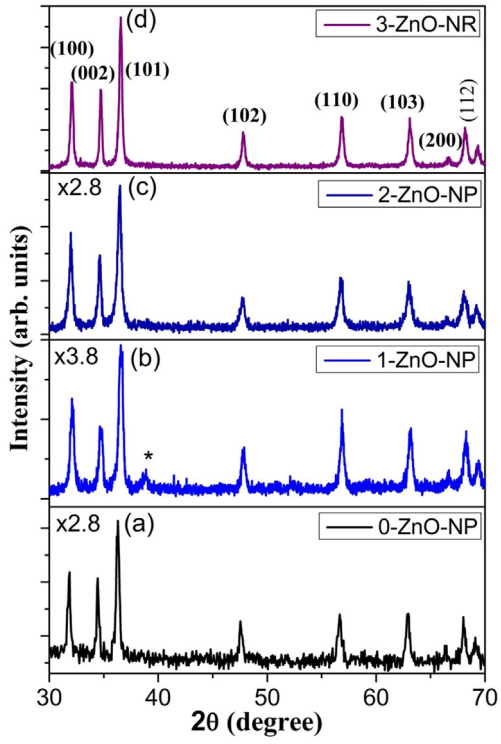

Fig. 1. (a–d) XRD pattern of $Zn_{1-x}Ni_xO$ (x = 0, 0.03, 0.05) samples, 0-ZnO-NPs, 1-ZnO-NPs, 2-ZnO-NPs, 3-ZnO-NRs respectively, showing wurtzite ZnO peaks. Doping induced peak shift is clearly seen for the intense peaks corresponding to (100), (002), and (101) planes. Details are mentioned in Table 1.

3.2. Local structure of dopant and defects

The valance state, substitution and elemental contents can be determined from the binding energies of each element by the XPS spectra analysis. The peak positions depend on the local structure of the different ions and can provide the information about the chemical state. Fig. 3 shows the XPS spectra of (1) Zn 2p, (2) Ni 2p and (3) O 1s states of pure and 3%, 5% Ni-doped ZnO NPs and NRs. Fig. 3(a–c) shows two strong peaks centered around 1021.54 eV and 1044.61 eV which are in agreement with the binding energies of Zn $2p_{3/2}$ and Zn $2p_{1/2}$ respectively for all the Ni doped samples. Their spin-orbital splitting energy is around 23.07 eV, confirming that Zn is present as Zn^{2+}.Fig. 3 (d–f) show that the peaks of Ni $2p_{3/2}$ and Ni $2p_{1/2}$ core levels are centered around 855.51 and 873.01 eV, respectively, whereas the corresponding satellite structures are clearly observed at 861.01 and 879.11 eV for all the Ni doped samples. The ionic state and the phase information of the Ni ions within the ZnO matrix can be explained on the basis of the energy difference between Ni $2p_{3/2}$ and Ni $2p_{1/2}$ core levels. For Ni^{2+} states inside ZnO matrix, the spin-orbital splitting energy difference is around 17.50 eV, which is different from the value (17.27 eV) of the metallic Ni phase [29,30]. We observe the spin-orbital splitting energy as 17.51 and 17.50 eV for the 2-ZnO and 3-ZnOsamples which show RT FM behavior. Whereas this energy difference is around 17.80 eV for the 1-ZnO sample which shows paramagnetic nature. This relative higher splitting energy is observed due to the presence of Ni related secondary phases, which is also evidenced from the XRD pattern. Also, observed Ni $2p_{3/2}$ (855.51 eV) position is quite different from that of the metallic Ni (852.7 eV), NiO (853.8 eV) and Ni_2O_3 (856.7 eV) [31]. Furthermore, the shape of peaks for Ni metallic with satellites structure is narrow and different from the observed spectrum of Ni-doped ZnO NPs [31]. These results provide clear evidence, that Ni ions are successfully substituted into tetrahedral sites of the ZnO wurtzite structure without forming any detectable secondary phases.

Fig. 3(g–i) show O1s peak for the Ni doped ZnO NPs, NRs. The binding energy peak at nearly 530 eV is attributed to O atoms at regular lattice site (O_L), between O^{2-} and Zn^{2+} (or substitutional Ni^{2+}) ions [32]. The small intensity peak at higher binding energy of 533 eV corresponds to interstitial O atoms (O_i) or surface oxygen in forms of –OH groups. Also we have shown the detail elemental analysis of Zn, O and Ni in Table 1, calculated from the XPS spectra. It indicates that the percentage O is higher in all the samples and thus presence of Zn vacancy (Zn_V) and O interstitials (O_i) are expected. Further, insertion of Ni ions inside ZnO matrix is more efficient around 3.9% for the 5% Ni doped ZnO NRs enhancing FM ordering, supporting the importance of higher concentration of doping with the axial accommodation.

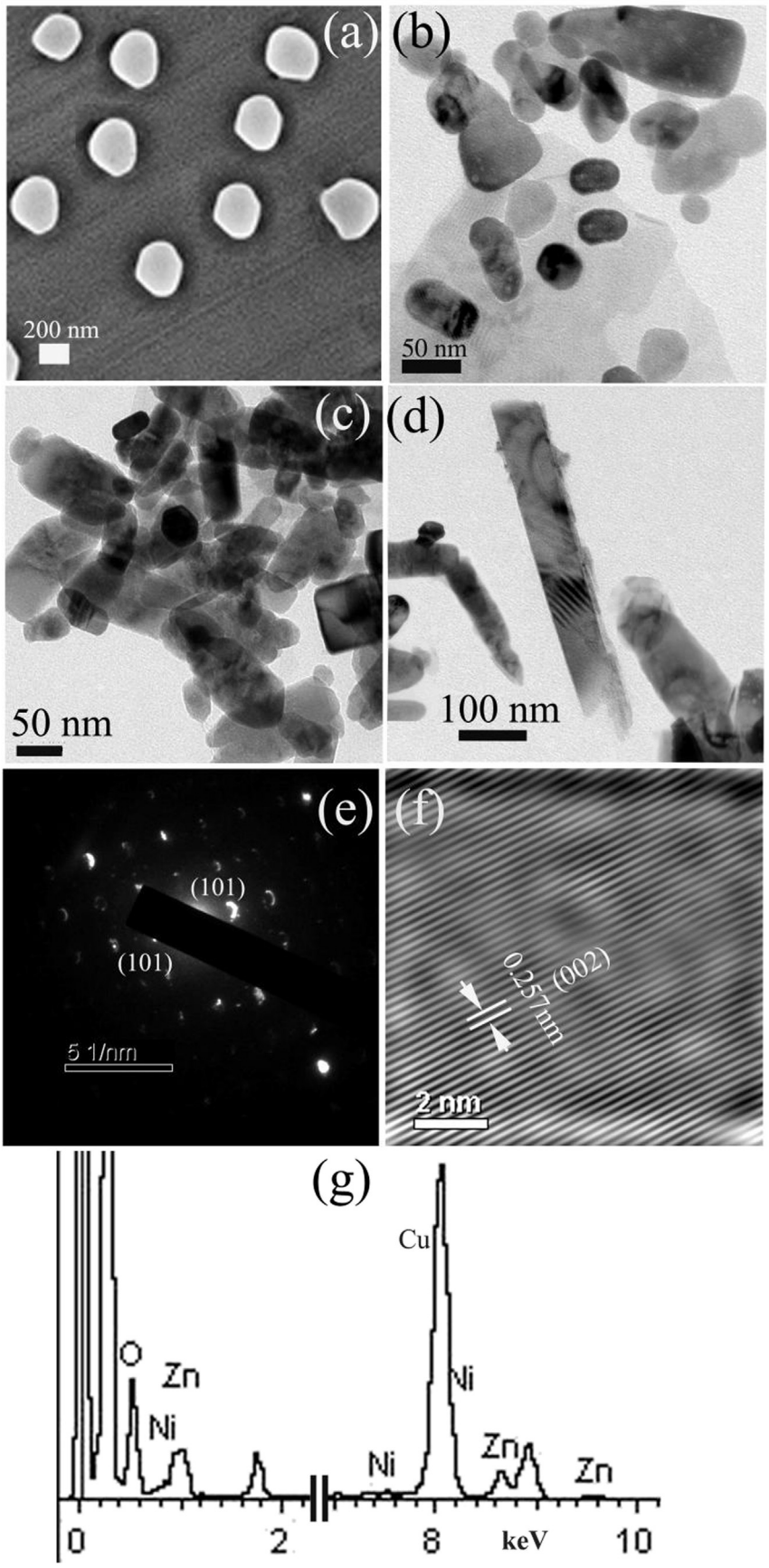

Fig. 2. (a) FESEM image of the undoped ZnO NPs. (b–c) TEM image of the 3% & 5% Ni doped ZnO NPs respectively (d) TEM image of the 5% Ni doped ZnO NRs, (e) SAED pattern & (f) HRTEM lattice image of the a single 5% Ni doped ZnO NR showing c-axis growth. (g) EDS spectra of a single Ni doped ZnO NRs, showing presence of Ni inside the ZnO lattice.

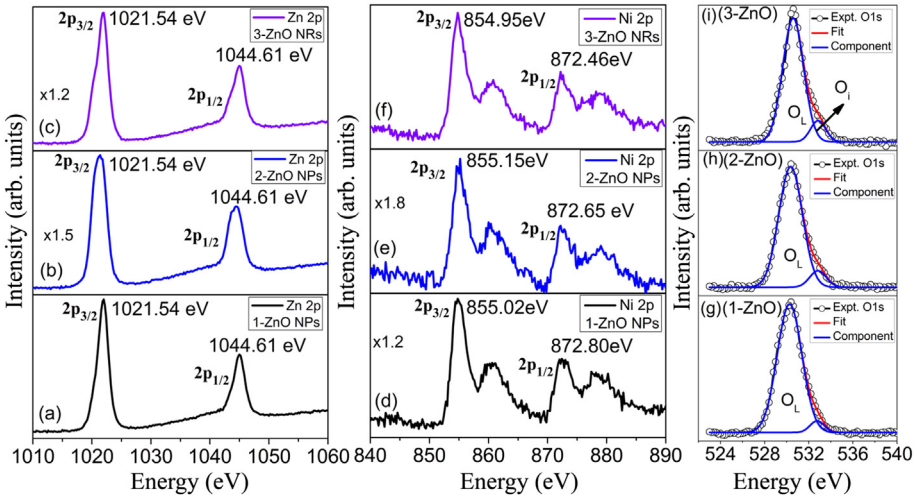

Fig. 3. XPS spectra of (a–c) Zn $2p_{3/2}$ and $2p_{1/2}$ states; (d–f) Ni $2p_{3/2}$ and $2p_{1/2}$ states; (g–i) O 1s statesof3%, 5% Ni doped ZnO NPs, NRs; (1-ZnO, 2-ZnO, 3-ZnO samples).

3.3. Optical properties

PL studies for the undoped and Ni doped ZnO samples at room temperature reveal strong UV emission peak and a broad green-yellow emission band ranging from 425 nm to 725 nm, as shown in Fig. 4(a–d). Observed broad PL peaks in the UV as well as in the visible region indicate existence of multicomponents which are extracted after fitting with multiple Gaussian functions. The obtained individual peak positions are tabulated in Table 2. Undoped ZnO NPs exhibit an excitonic emission band centered on 3.25 eV (Peak I). Ni-doped ZnO NPs, NRs show slight blueshift in the above mentioned UV emission. The near band-edge (NBE)transition is generally attributed to the recombination of free excitons. The blue shift of the UV emission peak has been attributed to the strong exchange interaction between the d-electrons of Ni ions and the s, p electrons of the host band. Along with the free excitonic UV emission, one additional peak (Pak II) centered at 3.15eVis observed from all of the samples near the tail region of the above UV emission. Band tail states are seen due to the surface effect of nanomaterials caused by the presence of lattice disorder/defects on the surface in the chemical synthesized ZnO nanostructures [33,34].

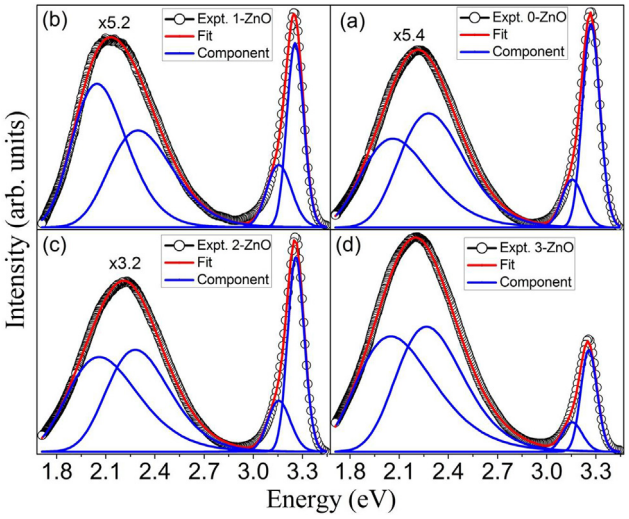

Fig. 4. (a–d) show PL spectra of undoped, 3%, 5% Ni doped ZnO NPs, NRs. Strong UV and visible PL bands related to defects can be seen due to presence of Zn_V, O_i, O_{Zn}, defects. Different PL peaks (I up to IV) are fitted with Gaussian functions and shown in Table 2.

Next, PL peak is the green emission peak (Peak III) centered on ~2.30–2.27 eV, which is commonly observed in the ZnO nanostructures. This broad peak in the visible region is well known for the intrinsic defects in ZnO, such as zinc vacancy (Zn_V) or Oxyzen vacancy (O_V) related defects [35–38] or antisite oxygen (O_{Zn}) [7]. Emre etal. also reported about Zn_V, O_V defects as the source of green luminescence through detail EPR analysis [39]. However as our samples are O rich, as evidenced from XPS and EDS analysis, the presence of O_V is expected to be very less. Thus origin of this peak is considered as the presence of Zinc vacancy (V_{Zn}) and or antisite oxygen (O_{Zn}). Next an intense yellow emission (Peak IV) is observed from all of the samples, centered on ~2.05 eV. This emission peak may be attributed to the recombination process associated with the ionized oxygen interstitials (O_i) induced transitions [35,40]. Most of the theoretical calculations agree that Zn_V and O_V are the lowest energy defects, while the Zn_i, O_i are to be higher in energy. Generally the defects which are favored under Zn-rich conditions (O_V, Zn_i) act as donors, while those favored under O-rich conditions (Zn_V, O_i) act as acceptors [7]. So the formation of Zn_V, O_i related defects are more expected in case of these chemical synthesized $Zn_{1-x}Ni_xO$ NPs, NRs. It is important to note that the position and the intensity of the defect related emission band strongly depend on the synthesis, as the origin as well as the concentration of intrinsic defects is in close relation with the synthesis procedure [38,41,42].

Note that the relative intensity of the defect emission to NBE emission has increased for the doped samples as compared to the undoped ZnO NPs. Also the overall defect density has increased for the doped NPs and NRs with increased C-axis growth. We can clearly see from the comparison of the PL intensity profile that the relative defect (V_{Zn}, O_i) band intensity has increased for the 5% Ni

Table 2
Summary of the PL peaks with UV and visible emission bands fitted with Gaussian line shapes.

Sample	Peak I (eV)	Peak II (eV)	Peak III (eV)	Peak IV (eV)
0-ZnO NPs	3.25	3.16	2.28	2.05
1-ZnO NPs	3.26	3.15	2.30	2.05
2-ZnO NPs	3.29	3.15	2.28	2.06
3-ZnO NRs	3.28	3.16	2.27	2.06
Peak identity	*NBE*	*Bandtail states*	Zn_V, O_{Zn}, V_0^+	O_i

doped NPs and NRs as compared to the undoped ZnO sample. High defect density with the higher percentage of doped Ni ions has chances of high density BMP formation, thus producing high magnetic moment through long range FM interaction [29,43]. We observe the appearance of RT FM characteristic in the Ni doped ZnO NRs with the presence of relative higher concentration of V_{Zn}, O_i defects. Whereas the Ni doped ZnO NPs with the presence of relative lower concentrations of defects shows PM or low moment of FM characteristic. It suggests that high concentration of V_{Zn}, O_i related defects along with the Ni ions inside ZnO matrix promote the FM interaction. Thus doping of Ni^{2+} ions also can be used to tune the visible PL properties of the ZnO nanostructures and this intern affects the magnetic properties of the doped ZnO NPs.

3.4. Magnetic properties

We observe distinct ferromagnetic behavior with high moment in the doped $Zn_{1-x}Ni_xO$ NRs measured by VSM. Fig. 5 (b–c) shows the magnetic hysteresis (M-H) loop for the 5% Ni doped ZnO NPs and NRs respectively measured at room temperature. Ni doped ZnO NPs synthesized for lower reaction temperature show weak FM characteristics with low moment, while Ni doped ZnO NRs synthesized for higher reaction temperature shows strong FM characteristics. Observed saturation magnetic moment (Ms) is of the order of 1.13 emu/g for the 5% Ni doped ZnO NRs. Detailed variation of the coercivity, retentivity and other magnetic properties are mentioned in the Table 3. It is well known that for the wide range of applications, the DMS material should have a Tc enough above RT (300 K). It's clear from the RT M-H loop that this material can retain FM characteristic far above room temperature, as a result Tc will be high. Note, that the magnetic moment value for the Ni doped ZnO NRs, as observed here, is relatively high as compared to the other findings for the Ni doped ZnO based DMS NRs/NWs [27,44]. But in general Ni doped ZnO nanostructure systems show lower magnetic moment as compared to the Co doped counterpart [45,46].

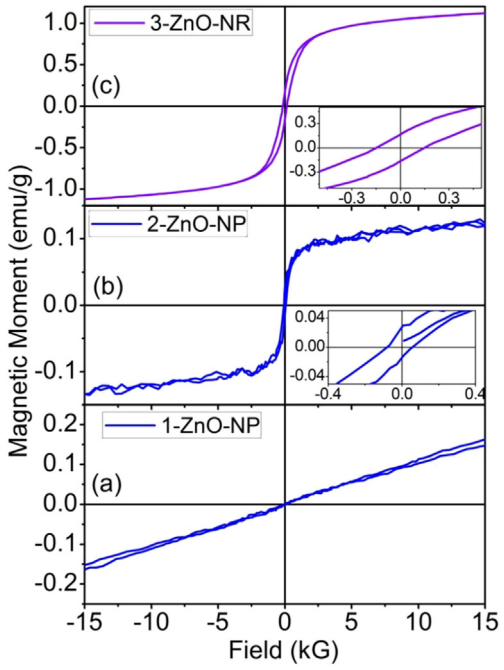

Fig. 5. (a–c) Room temperature M-H plot showing the hysteresis loop for the 3%, 5% Ni doped ZnO NPs, NRs. The inset shows the magnified M-H loop showing clear ferromagnetic hysteresis behavior for the NRs with higher reaction temperature and time.

While, Ni doped NPs synthesized for both lower reaction time and temperature we observe PM characteristic, as the substituted Ni concentration and defect concentration are low (Fig. 5 (a)). Also Ni related secondary phases are present. As the kind of magnetic interaction for the Ni related extrinsic phases and the Ni ions inside the ZnO matrix are different, as a result the overall magnetic moment is not favoring FM nature for the 1-ZnO NPs. As the relative concentration of Ni doping and defect density have increased, so it enhances stronger FM interaction through BMP formation. Also for the Ni doped ZnO NRs the axial accommodation of Ni ions is more favorable for the FM interaction, giving the higher value for FM moment [28,47]. We have observed in our earlier work of Co doped ZnO NRs the special importance of axial accommodation of TM ions in FM interaction [45]. Thus, the higher doping concentration, higher defect density and the 1D (NW/NR) growth of nanostructure might provide a better environment to yield FM interaction with high ordering temperature in solvothermal synthesis. Note that, despite the presence of intrinsic defects no measurable magnetic moment is observed in the undoped sample. This confirms that defects alone are not sufficient to account for the observed FM in case of as synthesized samples. Further, in our earlier work of Co doped (low concentration) ZnO NWs synthesized by vapor deposition, we found very low magnetic moment and its nature as PM, as the observed defect concentration was too low, hence the ferromagnetic coupling could not be favorable [48].

4. Possible origin of the FM interaction

Incorporation of the TM ions into the ZnO host lattice involves either the replacement of TM ions on regular Zn sites, or positioning on nonregular (i.e., interstitial) sites. The magnetic properties of the final system depend on many more parameters including the concentration and distribution of the TM ions, type and concentration of defects, n-type doping, p-type doping, morphology of the host lattice etc. Also on account of the nanostructure nature, the surface effects are very pronounced for the high surface-to volume ratio. There are two interacting subsystems in DMS materials: the delocalized conduction band electrons, valance band holes and the diluted system of localized magnetic moments associated with the TM ions. Ferromagnetic interaction couples the spins of s-like electrons or p-like holes near the band edges to the d-shell spins of the TM ions. The first proposed model was the Zener model driven by the exchange interactions between carriers and localized spins (s–d interaction) [49]. Later Dietl et al. have used the Zener description to realize possible origin of RT FM as hole-mediated exchange interactions and theoretically predicted a curie temperature above room temperature in p-type ZnO with 5% Mn atoms as dopants and a carrier concentration of 3.5×10^{20} holes cm^{-3} [1].

The presence of intrinsic defects (Zn_V, Zn_i, O_{Zn}, O_i etc.) play an important role in the FM interaction for Ni doped ZnO systems [35,50,51]. The long-range interaction is necessary to obtain HT FM in dilute concentration of Ni doped ZnO DMS systems and it can be mediated by defect induced states [6]. According to the bound magnetic polaron (BMP) model, bound electrons (holes) in the defect states can couple with TM ions and cause the ferromagnetic regions to overlap, giving rise to long range FM ordering [12,13]. When donors or acceptors are present, the sp-d interaction often leads to the formation of BMPs. A BMP is a particular type of complex near an occupied donor or an acceptor. It consists of the bound electron (hole) together with the spins of the TM ions within a hydrogenic Bohr orbit of radius r_H (for ZnO, $r_H = 0.76$ nm). Due to the sp-d interaction the latter spins can have a significant net

Table 3
Saturation magnetization (M_s), coercivity (H_c), and retentivity (M_r) determined from M-H curve; M_0, $m_{ef\,f}$, χ_m, N are determined from the BMP fitting of the M-H curves for different $Zn_{1-x}Ni_xO$ (x = 0, 0.03, 0.05) samples.

Sample type	M-H parameters			Fitting parameters extracted from BMP model			
	M_s (emu/g)	H_c(G)	M_r (emu/g)	M_0 (emu/g)	$m_{eff} \times 10^{-17}$ (emu)	$\chi_m \times 10^{-5}$ cg	$N \times 10^{17}$ (cm^{-3})
0-ZnO	…	…	…	…	…	…	…
1-ZnO	0.16	…	…	…	…	…	…
2-ZnO	0.20	70	0.02	…	…	…	…
3-ZnO	1.13	150	0.16	1.2	7.45	2.34	1.25

ferromagnetic alignment [13]. Percolation of BMPs promotes high magnetic moment and high Curie temperature. In an earlier work on Co doped ZnO NPs, NRs we have demonstrated the important role of BMPs to achieve HT FM with high moment for the ZnO based DMS system [45,52].

Intrinsic defects, such as Zn_V, O_i, O_{Zn} are inherently present in the as synthesized $Zn_{1-x}Ni_xO$ NRs due to the stabilization of structure. Zn vacancies promotes the FM ordering by affecting the occupancy of extended Ni ions, also the presence of holes with the V_{Zn} make $Zn_{1-x}Ni_xO$ NRs strongly FM, as O_i defects contribute holes in the above samples [53]. Further J.B. Yi have reported that Zn vacancies itself might introduce magnetic moments as well as additional holes and FM coupling of these local moments could be mediated by the high concentration of holes introduced by doping and defects, resulting in RTFM [53]. Our systematic study shows that formation of defect (V_{Zn}, O_i) mediated BMPs and their percolation is one of the most promising candidates for the observed FM. To understand the suitability of the BMP model, we attempt to fit the M versus H data using the BMP model [13]. The formula used for the fitting of BMP model:

$$M = M_0 L(x) + \chi_m H \quad (1)$$

The first term in represents the contribution of the BMP's, second term is the matrix contribution. Details of Eq. (1) are mentioned in earlier work [45]. The experimental data along with fitted data are shown in Fig. 6 for the 5% Ni doped ZnO NRs. The fitted data closely follows the experimental data and the fitted parameters are tabulated in Table 3. The spontaneous moment per BMP, m_{eff} is found to be of the order of 10^{-17} emu. By assuming $m_s = m_{eff}$, we have estimated the concentration of BMP to be of the order of 10^{17} cm^{-3} considering the effective Bohr radius of the BMPs as 0.76 nm.

The calculated BMP concentration is relatively small compared to the necessary concentration of 10^{20} cm^{-3} in order to have long range percolation. Thus, the calculated low concentration of BMPs cannot fully account for the observed high magnetic moment in the doped ZnO. Also defect related surface spins might contribute partly for the observed FM. Due to a large surface area, a lot of

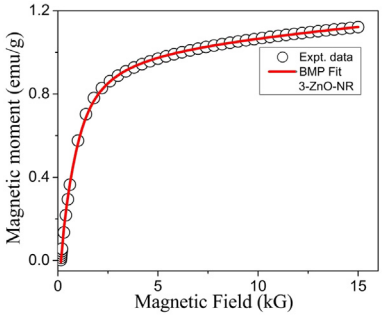

Fig. 6. Initial curve (0-H_{max}) of the M-H plot is fitted with BMP model (Eq. (1)) for the 5% Ni doped ZnO NRs. Symbols are for experimental data and the solid line is a fit with the BMP model. Extracted parameters are shown in Table 3.

defects have been seen in the PL and XPS spectra. Sanchez et al. have reported that the uncompensated surface spins enhance the spin polarization induced by substitute Ni ions and even in the absence of magnetic ions, it might promote the formation of p-derived extended magnetic states [54]. Further, presence of O_i, in our samples is favorable to exhibit presence of holes due to the activation of acceptor states [40]. The activation of acceptor states for hole formation might be partly responsible for the enhancement in HTFM in the Ni doped ZnO NRs, also it is consistent with the Dietl's prediction of hole mediated ferromagnetism in Mn doped ZnO system [1]. Note that, we don't find any measurable magnetization in the undoped ZnO NPs. Also, defect related FM moment reported in the literature for the undoped nanostructures is of much lower magnitude (of the order of 10^{-3} emu/g) as compared to doped DMSs [17,18,43]. We observed at least three orders of higher moment in the Ni doped ZnO NRs. Possibly, axial growth of the NRs with higher concentration of Ni ion accommodation along C-axis enhances the FM interaction. Thus, it appears that both TMs as well as defects are important ingredients to attain high moment as well as high T_c, as observed here. More detailed experimental work like might provide further insights into the origin of ferromagnetism in magnetically doped oxides and the possible way to improve its quality.

5. Conclusion sample

RTFM with high magnetic moment is reported in the $Zn_{1-x}Ni_xO$ NRs synthesized by a solvothermal route. The shape and size of the Ni doped ZnO NS have increased with increasing reaction temperature and time, leading to the C-axis 1D growth and stronger FM characteristic. TEM micrograph reveals the formation of long and uniform ZnO NRs with 60–70 nm diameters and 0.4–0.6 μm length. XRD, XPS, HRTEM and EDS analysis confirm the absence of Ni clusters in the doped NPs/NRs. XPS spectra also confirm the presence of Ni ions in 2 + states within host lattice. RT magnetic measurements exhibit FM behavior with moment of 1.13emu/g and coercivity of150 G. The structural, optical, and magnetic properties are sensitively changed for the incorporation of Ni^{2+} ions in the Zn^{2+} lattice site. PL and XPS spectra confirm the nature of defects (Zn_V, O_i) present in the doped and undoped samples. PL spectra also demonstratedoping induced modification in the band edge emission. These findings suggest that Ni^{2+} ions are successfully incorporated into the wurtzite lattice at the Zn^{2+} sites. Theobserved FM is explained on the basis of intrinsic exchange interaction of Ni ionsand Zn_V, O_i defects, both the Ni ions as well as defects are significant ingredients to attain high moment as well as high ordering temperature.

Acknowledgments

We thank CSIR for providing senior research fellowship and financial support through project grant (09/059(0050/2k13/EMR-I)) in carrying out this work. We also thank Central Instruments Facility (CIF), IIT Guwahati and Department of Electrical and

Electronic Engineering, Kobe University, Japan to accomplish part of this work.

References

[1] T. Dietl, H. Ohno, F. Matsukura, Hole-mediated ferromagnetism in tetrahedrally coordinated semiconductors, Phys. Rev. B 63 (2001) 195205.
[2] K.S.a.H. Katyama-Yoshida, First principles materials design for semiconductor spintronics, Semicond. Sci. Technol. 17 (2002) 367.
[3] S.J. Pearton, D.P. Norton, M.P. Mil, A.F. Hebard, J.M. Zavada, W.M. Chen, I.A. Buyanova, ZnO Doped with transition metal ions, electron devices, IEEE Trans. 54 (2007) 1040–1048.
[4] C. Klingshirn, J. Fallert, H. Zhou, J. Sartor, C. Thiele, F. Maier-Flaig, D. Schneider, H. Kalt, 65 years of ZnO research – old and very recent results, Phys. status solidi (b) 247 (2010) 1424–1447.
[5] F. Pan, C. Song, X.J. Liu, Y.C. Yang, F. Zeng, Ferromagnetism and possible application in spintronics of transition-metal-doped ZnO films, Mater. Sci. Eng. R: Reports 62 (2008) 1–35.
[6] M.H.F. Sluiter, Y. Kawazoe, P. Sharma, A. Inoue, A.R. Raju, C. Rout, U.V. Waghmare, First principles based design and experimental evidence for a ZnO-based ferromagnet at room temperature, Phys. Rev. Lett. 94 (2005) 187204.
[7] A. Janotti, C.G.V.d. Walle, Fundamentals of zinc oxide as a semiconductor, Reports Prog. Phys. 72 (2009) 126501.
[8] Q. Li, T.T. Shen, Z.K. Dai, Y.L. Cao, S.S. Yan, S.S. Kang, Y.Y. Dai, Y.X. Chen, G.L. Liu, L.M. Mei, Spin polarization of $Zn_{1-x}Co_xO$ probed by magnetoresistance, Appl. Phys. Lett. 101 (2012) 172405.
[9] M.D. McCluskey, S.J. Jokela, Defects in ZnO, J. Appl. Phys. 106 (2009) 071101.
[10] T. Dietl, Origin of ferromagnetic response in diluted magnetic semiconductors and oxides, J. Phys. Condens. Matter 19 (2007) 165204.
[11] S.J. Pearton, D.P. Norton, K. Ip, Y.W. Heo, T. Steiner, Recent progress in processing and properties of ZnO, Prog. Mater. Sci. 50 (2005) 293–340.
[12] J.M. Coey, M. Venkatesan, C.B. Fitzgerald, Donor impurity band exchange in dilute ferromagnetic oxides, Nat. Mater. 4 (2005) 173–179.
[13] G.H. McCabe, T. Fries, M.T. Liu, Y. Shapira, L.R. Ram-Mohan, R. Kershaw, A. Wold, C. Fau, M. Averous, E.J. McNiff Jr., Bound magnetic polarons in p-type Cu_{2}Mn_{0.9}Zn_{0.1}SnS_{4}, Phys. Rev. B 56 (1997) 6673–6680.
[14] S. Zhou, K. Potzger, J. von Borany, R. Grötzschel, W. Skorupa, M. Helm, J. Fassbender, Crystallographically oriented Co and Ni nanocrystals inside ZnO formed by ion implantation and postannealing, Phys. Rev. B 77 (2008) 035209.
[15] M. Snure, D. Kumar, A. Tiwari, Ferromagnetism in Ni-doped ZnO films: extrinsic or intrinsic? Appl. Phys. Lett. 94 (2009) 012510.
[16] Q. Xu, H. Schmidt, S. Zhou, K. Potzger, M. Helm, H. Hochmuth, M. Lorenz, A. Setzer, P. Esquinazi, C. Meinecke, M. Grundmann, Room temperature ferromagnetism in ZnO films due to defects, Appl. Phys. Lett. 92 (2008) 082508.
[17] D. Gao, Z. Zhang, J. Fu, Y. Xu, J. Qi, D. Xue, Room temperature ferromagnetism of pure ZnO nanoparticles, J. Appl. Phys. 105 (2009) 113928.
[18] S. Banerjee, M. Mandal, N. Gayathri, M. Sardar, Enhancement of ferromagnetism upon thermal annealing in pure ZnO, Appl. Phys. Lett. 91 (2007) 182501.
[19] X. Liu, F. Lin, L. Sun, W. Cheng, X. Ma, W. Shi, Doping concentration dependence of room-temperature ferromagnetism for Ni-doped ZnO thin films prepared by pulsed-laser deposition, Appl. Phys. Lett. 88 (2006) 062508.
[20] G. Srinet, R. Kumar, V. Sajal, Structural, optical, vibrational, and magnetic properties of sol-gel derived Ni doped ZnO nanoparticles, J. Appl. Phys. 114 (2013) 033912.
[21] P. Satyarthi, S. Ghosh, B. Pandey, P. Kumar, C.L. Chen, C.L. Dong, W.F. Pong, D. Kanjilal, K. Asokan, P. Srivastava, Coexistence of intrinsic and extrinsic origins of room temperature ferromagnetism in as implanted and thermally annealed ZnO films probed by X-ray absorption spectroscopy, J. Appl. Phys. 113 (2013) 183708.
[22] L.-N. Tong, X.-M. He, H.-B. Han, J.-L. Hu, A.-L. Xia, Y. Tong, Effects of annealing on ferromagnetism of Ni-doped ZnO powders, Solid State Commun. 150 (2010) 1112–1116.
[23] R.K. Singhal, S.C. Sharma, P. Kumari, S. Kumar, Y.T. Xing, U.P. Deshpande, T. Shripathi, E. Saitovitch, Study of electronic structure and magnetization correlations in hydrogenated and vacuum annealed Ni doped ZnO, J. Appl. Phys. 109 (2011) 063907.
[24] R.D. Shannon, Revised effective ionic-radii and systematic studies of interatomic distances in halides and chalcogenides, Acta Crystallogr. Sect. A 32 (1976) 751–767.
[25] W.-J. Li, E.-W. Shi, W.-Z. Zhong, Z.-W. Yin, Growth mechanism and growth habit of oxide crystals, J. Cryst. Growth 203 (1999) 186–196.
[26] J. Yang, M. Gao, L. Yang, Y. Zhang, J. Lang, D. Wang, Y. Wang, H. Liu, H. Fan, Low-temperature growth and optical properties of Ce-doped ZnO nanorods, Appl. Surf. Sci. 255 (2008) 2646–2650.
[27] H. Hao, M. Qin, P. Li, Structural, optical, and magnetic properties of Co-doped ZnO nanorods fabricated by a facile solution route, J. Alloy Compd. 515 (2012) 143–148.
[28] S. Shi, Y. Yang, J. Xu, L. Li, X. Zhang, G.-H. Hu, Z.-M. Dang, Structural, optical and magnetic properties of Co-doped ZnO nanorods prepared by hydrothermal method, J. Alloy Compd. 576 (2013) 59–65.
[29] J. Iqbal, B. Wang, X. Liu, D. Yu, B. He, R. Yu, Oxygen-vacancy-induced green emission and room-temperature ferromagnetism in Ni-doped ZnO nanorods, New J. Phys. 11 (2009) 063009.
[30] H. Wang, Y. Chen, H.B. Wang, C. Zhang, F.J. Yang, J.X. Duan, C.P. Yang, Y.M. Xu, M.J. Zhou, Q. Li, High resolution transmission electron microscopy and Raman scattering studies of room temperature ferromagnetic Ni-doped ZnO nanocrystals, Appl. Phys. Lett. 90 (2007) 052505.
[31] J.F. Moulder, W.F. Stickle, P.E. Sobol, K.D. Bomben, Handbook of X-ray photoelectron spectroscopy, 1992.
[32] M. Chen, X. Wang, Y.H. Yu, Z.L. Pei, X.D. Bai, C. Sun, R.F. Huang, L.S. Wen, X-ray photoelectron spectroscopy and auger electron spectroscopy studies of Al-doped ZnO films, Appl. Surf. Sci. 158 (2000) 134–140.
[33] Q.P. Wang, D.H. Zhang, Z.Y. Xue, X.T. Hao, Violet luminescence emitted from ZnO films deposited on Si substrate by rf magnetron sputtering, Appl. Surf. Sci. 201 (2002) 123–128.
[34] F. Zhao, J.-G. Zheng, X. Yang, X. Li, J. Wang, F. Zhao, K.S. Wong, C. Liang, M. Wu, Complex ZnO nanotree arrays with tunable top, stem and branch structures, Nanoscale 2 (2010) 1674–1683.
[35] J. Liu, S. Lee, Y.H. Ahn, J.-Y. Park, K.H. Koh, Tailoring the visible photoluminescence of mass-produced ZnO nanowires, J. Phys. D: Appl. Phys. 42 (2009) 095401.
[36] K. Vanheusden, W.L. Warren, C.H. Seager, D.R. Tallant, J.A. Voigt, B.E. Gnade, Mechanisms behind green photoluminescence in ZnO phosphor powders, J. Appl. Phys. 79 (1996) 7983–7990.
[37] A.F. Kohan, G. Ceder, D. Morgan, C.G. Van de Walle, First-principles study of native point defects in ZnO, Phys. Rev. B 61 (2000) 15019–15027.
[38] E. Erdem, Microwave power, temperature, atmospheric and light dependence of intrinsic defects in ZnO nanoparticles: A study of electron paramagnetic resonance (EPR) spectroscopy, J. Alloys Compd. 605 (2014) 34–44.
[39] R. Baraki, P. Zierep, E. Erdem, S. Weber, T. Granzow, Electron paramagnetic resonance study of ZnO varistor material, J. Phys. Condens. Matter 26 (2014) 115801.
[40] U. Ilyas, R.S. Rawat, T.L. Tan, P. Lee, R. Chen, H.D. Sun, L. Fengji, S. Zhang, Oxygen rich p-type ZnO thin films using wet chemical route with enhanced carrier concentration by temperature-dependent tuning of acceptor defects, J. Appl. Phys. 110 (2011) 093522–093527.
[41] H. Kaftelen, K. Ocakoglu, R. Thomann, S. Tu, S. Weber, E. Erdem, EPR and photoluminescence spectroscopy studies on the defect structure of ZnO nanocrystals, Phys. Rev. B 86 (2012) 014113.
[42] D. Li, Y.H. Leung, A.B. Djurišić, Z.T. Liu, M.H. Xie, S.L. Shi, S.J. Xu, W.K. Chan, Different origins of visible luminescence in ZnO nanostructures fabricated by the chemical and evaporation methods, Appl. Phys. Lett. 85 (2004) 1601–1603.
[43] Z.L. Lu, H.S. Hsu, Y.H. Tzeng, F.M. Zhang, Y.W. Du, J.C.A. Huang, The origins of ferromagnetism in Co-doped ZnO single crystalline films: from bound magnetic polaron to free carrier-mediated exchange interaction, Appl. Phys. Lett. 95 (2009) 102501.
[44] K. Ando, H. Saito, Z. Jin, T. Fukumura, M. Kawasaki, Y. Matsumoto, H. Koinuma, Magneto-optical properties of ZnO-based diluted magnetic semiconductors, J. Appl. Phys. 89 (2001) 7284–7286.
[45] B. Pal, S. Dhara, P.K. Giri, D. Sarkar, Room temperature ferromagnetism with high magnetic moment and optical properties of Co doped ZnO nanorods synthesized by a solvothermal route, J. Alloy Compd. 615 (2014) 378–385.
[46] B. Pal, P.K. Giri, Room temperature ferromagnetism in Co-doped ZnO nanoparticles: milling time dependence and annealing effect, Int. J. Nanosci. 10 (2011) 307–311.
[47] E.-C. Lee, K.J. Chang, Ferromagnetic versus antiferromagnetic interaction in Co-doped ZnO, Phys. Rev. B 69 (2004) 085205.
[48] B. Pal, S. Dhara, P.K. Giri, Co-doped ZnO nanowires grown by vapor–liquid–solid method: structural, optical and magnetic studies, Nano 07 (2012) 1250028.
[49] C. Zener, Interaction between the d-shells in the transition metals. III. Calculation of the Weiss factors in Fe, Co, and Ni, Phys. Rev. 83 (1951) 299–301.
[50] H. Ren, G. Xiang, G. Gu, X. Zhang, Enhancement of ferromagnetism of ZnO: Co nanocrystals by post-annealing treatment: the role of oxygen interstitials and zinc vacancies, Mater. Lett. 122 (2014) 256–260.
[51] S. Ghosh, G.G. Khan, A. Ghosh, S. Varma, K. Mandal, Zinc vacancy-induced high-TC ferromagnetism and photoluminescence in group-1 alkali-metal substituted p-type ZnO thin films, CrystEngComm 15 (2013) 7748–7755.
[52] B. Pal, P.K. Giri, High temperature ferromagnetism and optical properties of Co doped ZnO nanoparticles, J. Appl. Phys. 108 (2010) 084322.
[53] J.B. Yi, C.C. Lim, G.Z. Xing, H.M. Fan, L.H. Van, S.L. Huang, K.S. Yang, X.L. Huang, X.B. Qin, B.Y. Wang, T. Wu, L. Wang, H.T. Zhang, X.Y. Gao, T. Liu, A.T.S. Wee, Y.P. Feng, J. Ding, Ferromagnetism in dilute magnetic semiconductors through defect engineering: Li-doped ZnO, Phys. Rev. Lett. 104 (2010) 137201.
[54] N. Sanchez, S. Gallego, M.C. Muñoz, Magnetic states at the oxygen surfaces of ZnO and Co-doped ZnO, Phys. Rev. Lett. 101 (2008) 067206.